*Mindanao Journal of Science and Technology / Vol. 20 (Special Issue 1) (2022) 69-86*

# Numerical Analysis of Algebraic Flux Model using OpenFOAM in Differentially-heated Cavity Configurations

Ralph Carlo Evidente
Division of Advanced Nuclear Engineering
Pohang University of Science and Technology
Pohang, Gyeongbuk 37673 Republic of Korea
*ralphcarlo@postech.ac.kr*

Date received: January 2, 2021
Revision accepted: September 7, 2021

## Abstract

*The analysis of the turbulent natural convection is mathematically described by the equations of conservation of mass, energy and momentum. Closing these equations requires modeling turbulent momentum stress and turbulent heat flux using the k-omega Shear Stress Transport Model and Algebraic Flux Model (AFM), respectively. The Reynolds Averaged Navier-Stokes (RANS) methodological setup for an incompressible buoyancy-driven flow has a great potential in modeling the oxide layer of corium for the improvement of in-vessel melt retention-severe accident management guidelines (IVR-SAMG). However, the procedure also requires validation study from experimental data that also exhibit similar flow and thermal behavior. This paper presents the modeling of natural convection in a differentially-heated cavity configuration using standard turbulent heat flux approaches and modified AFM versions using OpenFOAM – an open-source C++-based software. Results showed an improvement of near-wall behavior with up to the thermal boundary thickness of 0.2 m from the heated wall by using AFM as compared with other approaches. Also, sensitivity analysis at varying coefficients in AFM was performed to assess its contribution to heat and fluid phenomena. It was demonstrated that the production term due to the non-uniformity of mean thermal field was highly sensitive up to a factor of 0.60 for buoyant and stratified conditions when AFM was incorporated in RANS approach.*

***Keywords***: algebraic flux model, RANS, turbulent heat flux, turbulent natural convection

## 1. Introduction

Over the past decades, many researchers have been focusing on the area of preventing severe accidents in nuclear power plants, which have notable impacts on the environment. Severe accidents in a nuclear reactor, such as the ones that occurred at Three-Mile Island, Chernobyl and Fukushima, are defined as conditions more severe than design basis accidents, which feature significant degradation of the reactor core (Whang *et al.*, 2019). One of its causes is the long absence of core cooling that results in overheating and the possible relocation of the melt pool to the lower plenum of the reactor vessel. Corium, the molten mixture, can be stratified with a metallic layer coming from debris particles of the reflector, steel, iron and zircaloy above an oxide layer, which is made up of $ZrO_2$ and $UO_2$. In these layers, heat transfer phenomena and fluid behavior play a vital role in vessel integrity. One of which is natural convection involving an internal heat source. The complexity of phenomena, occurring inside the corium, requires high-fidelity numerical simulation as various computational fluid dynamics (CFD) researchers considered the unsteadiness of the flow, near-wall modeling, the constant transition of the boundary layer regions and the turbulent kinetic energy production due to the buoyancy (Ma *et al.*, 2016).

Several experiments involving turbulent natural convection phenomena have been used to validate the simulation results. Cheesewright *et al.* (1986) considered the natural convection boundary layer in a rectangular cavity filled with air and having an aspect ratio of 5:0. Numerical validation involving this experimental study commonly utilizes the Reynolds Average Navier-Stokes (RANS) turbulence models to estimate flow details and local heat transfer for complex flows. In general, turbulent heat flux (THF) is calculated, depending on various circumstances, using any of the following: Simple Gradient Diffusion Hypothesis (SGDH), General Gradient Diffusion Hypothesis (GGDH) and Algebraic Flux Model (AFM).

Simulation results using SGDH have been reported to yield inaccurate solutions for natural convective flows since THF only depends on the temperature gradient. Meanwhile, GGDH is used for conditions involving shear dominant flows but not for strongly stratified natural convective flows. AFM requires another transport equation and may cause a higher computational cost. However, it has been pragmatic for buoyancy-driven and stratified flow conditions, thereby giving more accuracy and stability to model the thermal behavior of an enclosed system (Choi *et al.*, 2004; Shams, 2018). AFM for the turbulent heat flux calculation was previously validated using two-dimensional air-filled rectangular and square configuration to investigate its accuracy and stability. However, its performance depended strongly on the constants of the algebraic expression for each turbulence model (Choi *et al.*, 2004; Choi and Kim, 2006). Thus, many CFD researchers have still reported that convergence using advanced models was hardly achievable. Hence, further study is necessary to capture the turbulence and thermal phenomena near and away from the wall (Vieira *et al*., 2013).

Some CFD researchers have attempted to modify the AFM equations. The first notable AFM equation is the AFM-2005 equation, which was derived to account for thermal, mechanical and gravitational production terms necessary to capture turbulence energies (Hanjalić, 2002). It was originally developed for natural convection flow regime for unity Prandtl fluids by using an implicit, non-linear set of algebraic equations, assuming negligible advection and diffusion of the scalar flux in terms of mean flow quantities. Meanwhile, for non-unity Prandtl fluids and different flow regimes, a modification was done in a slender geometry with a 1:8 aspect ratio to calibrate the magnitude related to thermal and gravitational production terms, thereby changing their coefficients $Ct_1$ and $Ct_3$ as these give sensitivity in scenarios involving forced convection and natural convection, respectively (Shams *et al*., 2014; Shams, 2018).

To date, only a few CFD studies have been conducted regarding the individual contribution of coefficient values in differentially-heated cavity cases. The flow and thermal behavior in the said configuration play a significant role in estimating the turbulent convection phenomena of the oxide layer in the corium, which necessitates computational analysis using advanced models. Thus, this study aimed to implement AFM in the chosen CFD solver and validate it against the experimental data and depict its flow behavior using global, turbulent and heat flux parameters. More specifically, this study compared AFM with standard cases from the latest and modified versions and assessed coefficient sensitivity to airflow and thermal behavior.

## 2. Methodology

### *2.1 Governing Equations*

The analysis of the turbulent natural convection was mathematically described by the equations of conservation of mass, energy and momentum. RANS methodology was utilized for solving these equations involving incompressible buoyancy-driven flow. Assuming Boussinesq approximation that is the density of the fluid remains constant at all grid points, governing equations for this study are the Equations 1, 2 and 3.

$$\frac{\partial U_i}{\partial x_i} = 0 \tag{1}$$

$$\frac{\partial T}{\partial t} + U_j \frac{\partial T}{\partial x_i} = \frac{\partial}{\partial x_j}\left(\alpha \frac{\partial T}{\partial x_j} - \overline{\theta u_j}\right) \tag{2}$$

$$\frac{\partial U_i}{\partial t} + U_j \frac{\partial U_i}{\partial x_j} = -\frac{\partial P}{\partial x_i} + \frac{\partial}{\partial x_j}\left[\upsilon\left(\frac{\partial U_i}{\partial x_j} + \frac{\partial U_j}{\partial x_i}\right) - \overline{u_i u_j}\right] + \beta(T - T_o)g_i \tag{3}$$

where $U_i$ is a component of mean velocity and $T$ *is* the mean temperature. Both the turbulent stress ($\overline{u_i u_j}$) and turbulent heat flux ($\overline{\theta u_j}$) represent the unresolved turbulence contributions, which need to be modeled to close the above equations (Choi and Kim, 2006). Here, $\alpha$ is the thermal diffusivity, $\beta$ is the thermal expansion coefficient and $T_o$ is the initial temperature set for each wall condition.

The turbulent stress ($\overline{u_i u_j}$) was given by the Boussinesq hypothesis (Equation 4).

$$\overline{u_i u_j} = \upsilon_T \frac{\partial U_i}{\partial x_j} + \frac{2}{3} k \delta_{ij} \tag{4}$$

where $k$ is turbulence kinetic energy, $\upsilon_T$ is turbulent eddy viscosity and $\delta_{ij}$ is Kronecker delta, which can be modeled using $k - \omega$ shear stress (SST) transport equations. Previous studies showed that its turbulence performance can capture physics phenomena near and away from the wall due to its blending function (Davidson, 2021).

On the other hand, THF ($\overline{\theta u_i}$) in this study was modeled using AFM from Equations 5 to 8 (Kenjeres, 1998; Hanjalić, 2002).

$$\overline{\theta u_i} = -C_{t0} \frac{k}{\varepsilon}\left(C_{t1} \overline{u_i u_j} \frac{\partial T}{\partial x_j} + C_{t2} \overline{\theta u_j} \frac{\partial U_i}{\partial x_j} + C_{t3} \beta g_i \overline{\theta^2}\right) + C_{t4} a_{ij} \overline{\theta u_j} \tag{5}$$

$$\frac{\partial \overline{\theta^2}}{\partial t} + U_J \frac{\partial \overline{\theta^2}}{\partial x_j} = -2\overline{\theta u_j} \frac{\partial T}{\partial x_j} - 2\varepsilon_\theta + \frac{\partial}{\partial x_j}\left[\left(\upsilon + \frac{\upsilon_t}{\sigma_{\overline{\theta_2}}} \frac{\partial \overline{\theta^2}}{\partial x_j}\right)\right] \tag{6}$$

$$\varepsilon_\theta = \frac{\varepsilon\overline{\theta^2}}{2Rk} \tag{7}$$

$$R = \frac{\tau_{th}}{\tau_m} \approx 0.5 \tag{8}$$

where $a_{ij}$ is the stress-anisotropy tensor, $\overline{\theta^2}$ is the temperature variance, $\varepsilon_\theta$ is its dissipation and $R$ is the thermal-to-mechanical time-scale ratio. In this first part of the study, coefficients used in AFM equations (Table 1) were adopted from the reference, which is suitable for low-Reynolds turbulent natural convection (Kenjeres, 1998).

Table 1. Coefficients applied in Equation 5

| | $Ct_0$ | $Ct_1$ | $Ct_2$ | $Ct_3$ | $Ct_4$ |
|---|---|---|---|---|---|
| Air | 0.15 | 0.6 | 0.6 | 0.6 | 1.5 |

*2.2 Initial and Boundary Conditions*

A 2D rectangular air cavity with an aspect ratio of 5:1, as well as its wall boundary condition, was used in the numerical simulation (Figure 1).

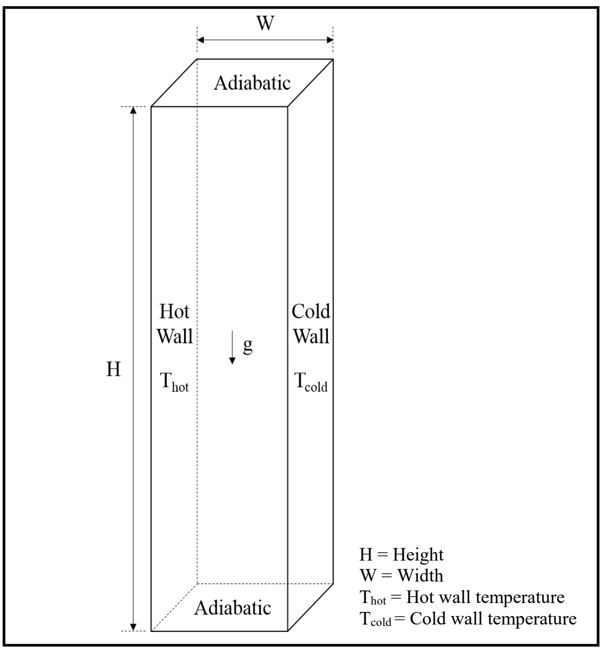


Figure 1. Geometrical configuration

One may state that the physics of natural convection heat transfer in internally heated liquid pools is geometry independent (Dinh and Nourgaliev, 1997). Thus, the database on cavities could be used for hemispherical cavities and vice versa. Also, the characteristics of turbulence models were intended to compare with the widely used and representative natural convection experiment, differentially-heated cavity (Cheesewright *et al.*, 1986).

Other parameters and constant values used in this study for the initial condition can be found in Table 2 and were implemented in open-source CFD C++ code, OpenFOAM version 2.3.1, whose numerical approach is based on the collocated finite volume method and solved in segregated matrices within an iterative sequence. The boundary conditions at solid walls were calculated by means of first cell center values of turbulent kinetic energy from the wall.

Table 2. Initial and boundary conditions

| Parameter | Initial condition |
|---|---|
| Simulant | Air |
| Rayleigh number (Ra = $Gr \times Pr$) | $5.2 \times 10^{10}$ |
| Grashof number (Gr = $g\beta\Delta TL^3/\upsilon^2$) | $7.4 \times 10^{10}$ |
| $T_{hot}$ / $T_{cold}$ ($\Delta T$) | 339.15 K/295.35 K (43.8 K) |
| Kinematic viscosity ($\upsilon$) | $1.73 \times 10^{-5}$ m²/s |
| Thermal expansion coefficient ($\beta$) | $3.15 \times 10^{-3}$ (1/K) |
| Prandtl number (Pr = $\nu/\alpha$) | 0.7 |
| No slip-condition | $U_i = 0$ |
| Reynolds stress | $\overline{u_i u_j} = 0$ |
| Turbulent heat flux | $\overline{\theta u_j} = 0$ |
| Temperature variation | $\overline{\theta^2} = 0$ |
| Wall dissipation | $\varepsilon_w = 2\nu k/x_j^2$ |

A maximum dimensionless height value ($y^+$) was 4.5 (Figure 2), which was measured along the hot wall. The generated graph was based on the mesh geometry; the monitored maximum $y^+$ value was anchored on the recommended dimensionless height values for SST-based models. It is noteworthy that regardless of the approaches of THF, the SST turbulence model was employed in all cases and so was the mesh geometry. Before this, mesh sensitivity analysis was checked before its application to work. The Semi-Implicit Pressure-Linked Equations (SIMPLE) algorithm was utilized for coupling the momentum and mass conservation equations suitable for steady-state calculations. For spatial discretization of the gradient, Laplacian and turbulent terms, the second-order accurate central differencing scheme was used. Meanwhile, the first-order accurate upwind scheme was employed for the treatment of convection terms.

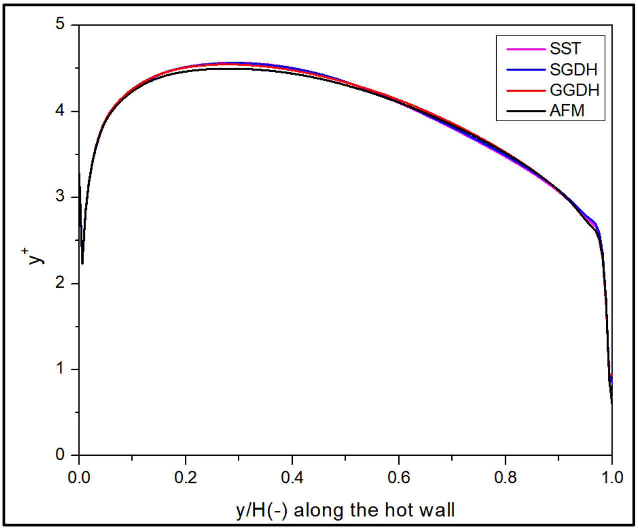


Figure 2. Dimensionless height generated from mesh

*2.3 Test Cases and Analyses*

The behavior from AFM computations was compared along with the standard approaches for turbulent heat flux as seen in Table 3. The SST plot was solved using solver buoyantBoussinesqSimpleFoam and was included solely for validation purposes against the results of SGDH-implemented simulation. Likewise, GGDH and AFM were both implemented based on the equations from the reference (Hanjalić, 2002).

Table 3. Treatment of THF

| Approach | Equation |
|---|---|
| SGDH | $\overline{\theta u_i} = -\frac{\upsilon_T}{Pr_T}\frac{\partial T}{\partial x_i}$ |
| GGDH | $\overline{\theta u_i} = -C_0\frac{k}{\varepsilon}(C_1\overline{u_i u_j}\frac{\partial T}{\partial x_j})$ |

The second part of the study (Table 4, Equations 9 and 10) incorporated the modified and calibrated versions of AFM, which the researcher named after the company's name (Nuclear Research and Consultancy Group [NRG]: NRG and NRG+) to the differentially-heated cavity case scenario (Shams, 2018). In Shams *et al.*'s (2004) study, the magnitude of the thermal production term showed dependency on Reynolds and Prandtl numbers in all flow scenarios involving unity and low Prandtl fluids such as air and liquid metals. To account for the temperature gradient normal to the wall as well as its fluid property (i.e., Prandtl number), NRG was applied to all flow regimes up to Ra of $10^6$. It was further calibrated to NRG+ and was applicable up to Ra of $10^{17}$. The said range was manifested to $C_{t3}$ correlation, where $a_1$ = -4.5 x $10^{-9}$, $a_2$ = 2.5 and n = 7. Both NRG and NRG+ use a logarithmic correlation and are sensitive to Reynolds and Rayleigh numbers, respectively. Based on the previous calibration studies, $C_{t1}$ and $C_{t3}$ gave sensitivity effect to forced and mixed/natural convection scenarios, respectively (Shams, 2018). From its logarithmic function of Re and Ra, the third analysis utilized a wide range of values of $C_{t1}$ and $C_{t3}$ as seen in the optimized and case models in Table 4 to account for its individual contribution, and varied (1) $C_{t0}$ and $C_{t1}$, and (2) $C_{t2}$ and $C_{t3}$ to determine the sensitivity of production terms to its near-wall characteristics.

Table 4. Treatment of modified THF approaches

| Model | $C_{t0}$ | $C_{t1}$ | $C_{t2}$ | $C_{t3}$ |
|---|---|---|---|---|
| AFM-2005 | 0.15 | 0.6 | 0.6 | 0.6 |
| AFM-NRG | 0.2 | Equation 9 | 0.6 | 2.5 |
| AFM-NRG+ | 0.2 | 0.25 | 0.6 | Equation 10 |
| Optimized | 0.2 | 1.0 | 0.6 | 1.5 |
| Case 1 | 0.1 | 0.2 | 0.6 | 1.5 |
| Case 2 | 0.1 | 0.6 | 0.6 | 1.5 |
| Case 3 | 0.3 | 1.0 | 0.6 | 1.5 |
| Case 4 | 0.2 | 1.0 | 0.4 | 0 |
| Case 5 | 0.2 | 1.0 | 0.8 | 2.5 |

$$C_{t_1} = 0.053 \ln \left(Re \cdot Pr\right) - 0.27 \tag{9}$$

$$C_{t_3} = a_1 \cdot \log_n (Ra \cdot Pr) + a_2 \tag{10}$$

## 3. Results and Discussion

### *3.1 Using Standard Cases*

Contour resulting images for global parameters, which can be seen in Figure 3, were well-matched with the temperature and velocity profile in Figures 4a and 4b. Edged-like peak behavior was apparent for the vertical velocity profile (Figure 4a). The significant differences can be observed starting from the peak (x/W = 0.05) until before the plots got dampened at x/W = 0.25. GGDH and AFM laid at the same apex. On the other hand, SGDH yielded the maximum point. All case models over-predicted the experimental data. For temperature profile, AFM was noticeable among other cases as depicted above and below of the theoretical mean temperature line.

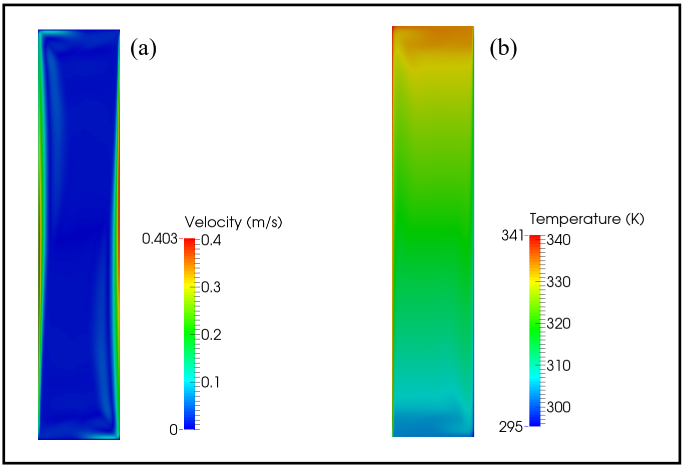


Left and right walls were considered hot and cold walls, respectively.

Figure 3. Contour plots with velocity (a) and temperature (b)

The temperature contour of the cavity in all cases showed that the airflow inside the cavity was strongly stratified due to asymmetrical boundary conditions of hot and cold walls, which gave a linear temperature gradient in the core region along the vertical height. Figure 4b, however, shows a slightly decreased gradient near the hot wall region. Meanwhile, Figure 4a exhibits that at the center region of mid-height, there was a least motion due to the effects of the upstream and downstream close to the hot and cold walls (Ji, 2014; Choi *et al*., 2017).

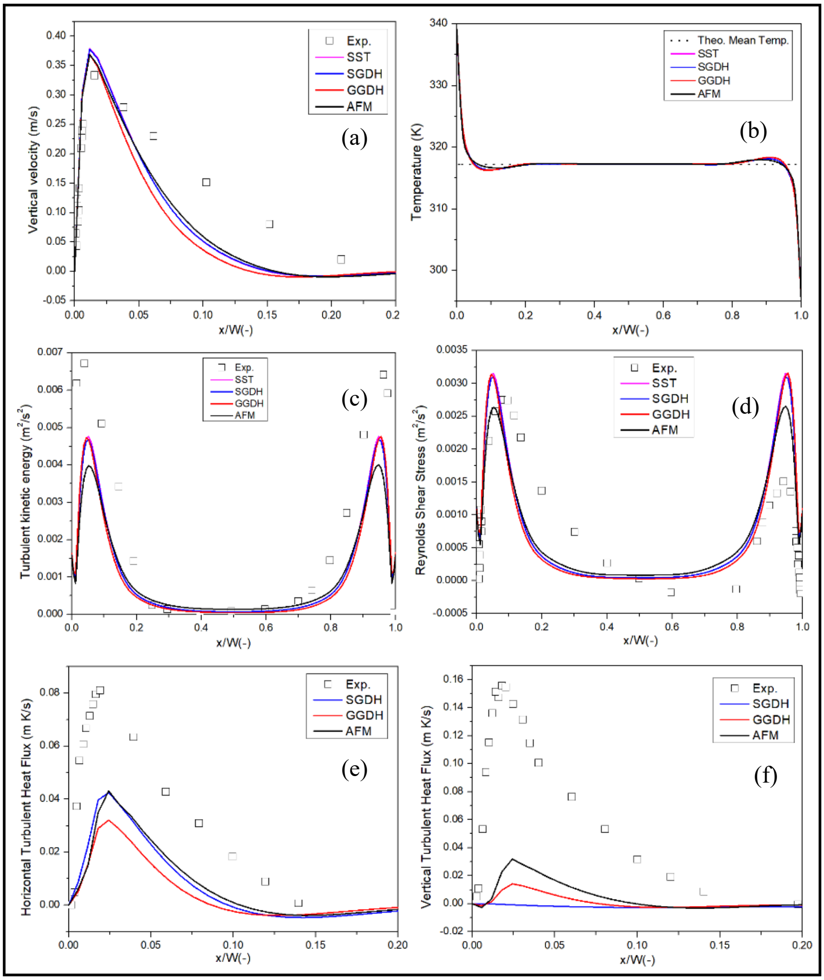

Figure 4. Vertical velocity (a), temperature (b), turbulent kinetic energy (c), Reynolds shear stress (d), horizontal (e) and vertical turbulent heat flux (f) measured through the mid-width (y/H = 1.25) of the cavity

Regarding the differences of numerical results and experimental plots of turbulence parameters (i.e., turbulent kinetic energy and Reynolds shear stress) in Figures 4c and 4d, it was reported difficult to establish a perfectly insulated boundary in the experiment, and thus generated asymmetric flows (Cheesewright *et al*., 1986). It was partly because of imperfect insulation at the ceiling of the cavity, where the small amount of heat loss prohibits the flow from relaminarization; hence, the latter took place at the bottom of the cavity. The simulation results indicated that AFM was under-predicted by other case models. Distinguished gaps can be perceived starting from the peak until its dampening behavior, with AFM giving the higher values followed by SGDH and GGDH, respectively. The lower values of AFM in the boundary thickness layer can be attributed to its dissipation – faster compared with the standard cases, thereby decreasing turbulence intensity values (Peng and Davidson, 1999).

Meanwhile, as seen in Figures 4e and 4f, sharp-edged peaks in the generated THF plots (seen in x/W = 0.025), despite using high resolution, were depicted in the maxima behavior of all cases. A similar tendency was observed in AFM and SGDH for the horizontal turbulent heat flux, while AFM produced a maximum peak for vertical turbulent heat flux similar to the study of Kenjeres (1998). If one would take closely in the plot of vertical THF, AFM gave hollow-like minima behavior before it reached the center of mid-width (Vieira *et al.*, 2013). As expected, SGDH's profile was flat due to the negligible streamwise gradient, whereas AFM's relative performance can be credited to the addition of three production terms particularly on the buoyancy production term designed for turbulent natural convection scenarios. Choi *et al.* (2017) further explained that the underprediction of vertical turbulent heat flux plays a significant role in the overall evaluation of other quantities. It can either be improved by a finer mesh in the near-wall or by tuning the coefficients of the AFM equation.

*3.2 Using Modified Versions*

As seen in Equation 5, each coefficient was directly proportional to the magnitude of turbulent heat flux or individual production term. $C_{t0}$ is a coefficient that determines the magnitude of the turbulent heat flux, and $C_{t1}$, $C_{t2}$ and $C_{t3}$ are coefficients that regulate the magnitude of the thermal, mechanical and gravitational production term, respectively. As the coefficient increases, overall turbulent flux increases such as turbulent stresses and turbulent heat fluxes. On the contrary, when the coefficient becomes small, the overall turbulence intensity becomes weak and the turbulence value turns out to be zero (predicting laminar flow for the entire computational domain) in some cases.

As a first step, NRG and NRG+ were tested in a differentially-heated cavity case. Using direct numerical simulation (DNS) data of wavy-wall channel flow, these modified equations were results of the calibration of AFM-2005 to improve prediction capabilities for natural, mixed and forced convection flows at low Prandtl numbers (Shams *et al.*, 2014). $C_{t1}$ and $C_{t3}$ of NRG and

NRG+ were evaluated as 0.005 and 2.5, respectively. In Figure 5, AFM-2005 still gave higher turbulent heat flux values for the differentially-heated cavity (DHC) case. NRG+ offset between AFM-2005 and NRG, $C_{t1}$ was highly sensitive for turbulent heat flux. This means that the thermal production term, with its proportionality to temperature gradient, dictates the overall behavior, and is mostly appropriate for buoyant and stratified conditions.

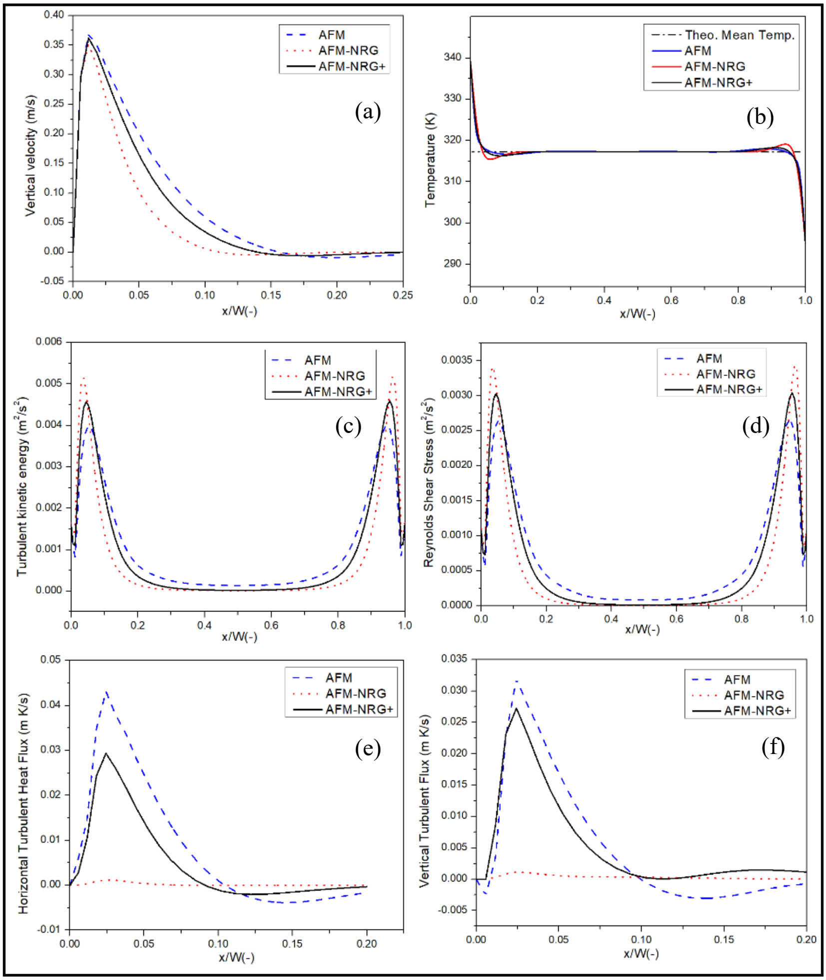


Figure 5. Effects of calibrated AFM equations to the evaluated parameters (vertical velocity [a], temperature [b], turbulent kinetic energy [c], Reynolds shear stress [d], horizontal [e] and vertical turbulent heat flux [f]) measured through the mid-width (y/H = 1.25) of the cavity

### *3.3 Sensitivity Effect*

A follow-up sensitivity analysis was performed to determine the effect of varying the magnitude of the production terms to the evaluated parameters. Moreover, optimized coefficients for the DHC air case had been evaluated as a result of the parameter study using a wide range of coefficients. Figures 6 to 9 compared the effect of each coefficient on the flow and thermal characteristics in DHC.

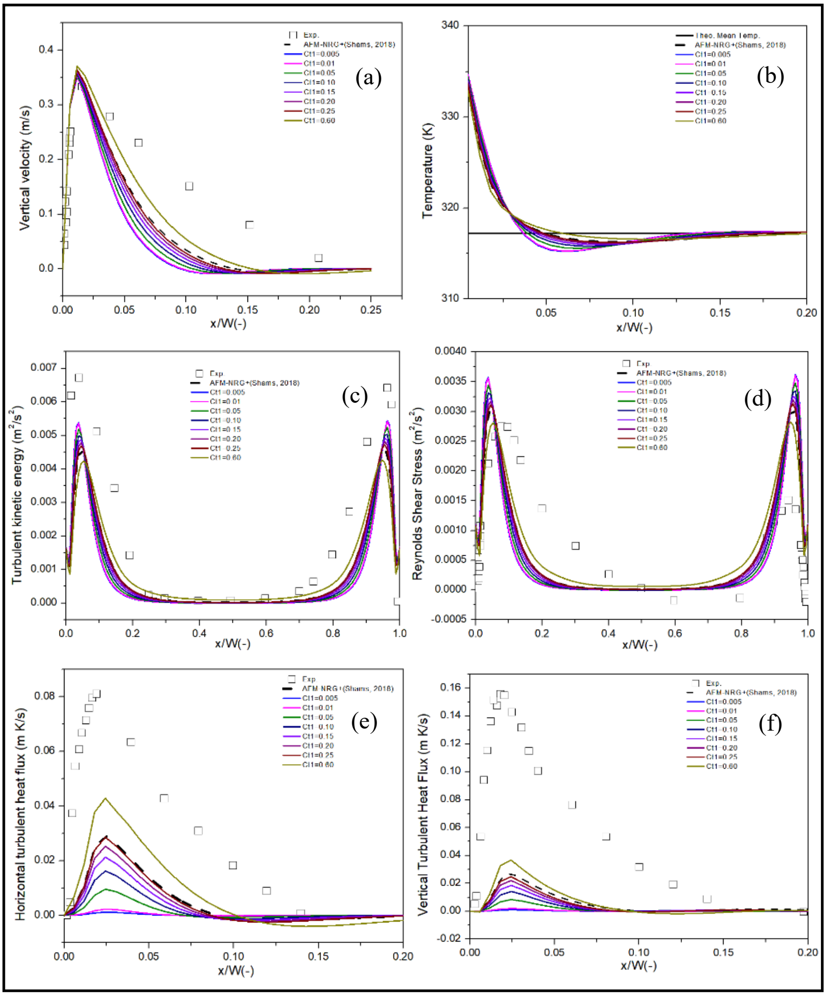

Figure 6. Sensitivity effect of $C_{t1}$ to the to the evaluated parameters (vertical velocity [a], temperature [b], turbulent kinetic energy [c], Reynolds shear stress [d], horizontal [e] and vertical turbulent heat flux [f]) measured through the mid-width (y/H = 1.25) of the cavity

Square symbols were experimental data; a solid line showed the result using optimized coefficients or AFM-NRG+; other colored lines displayed the result using an adjusted coefficient. Concerning the effect of $C_{t1}$, as the coefficient increased, the plot of velocity profile shifted to the right and gradient transition behavior became lesser (Figure 6). Turbulent heat flux increased, while turbulent intensity decreased. A slight increase of turbulent intensity and heat flux was observed in the sensitivity effect of increasing $C_{t3}$ (Figure 7).

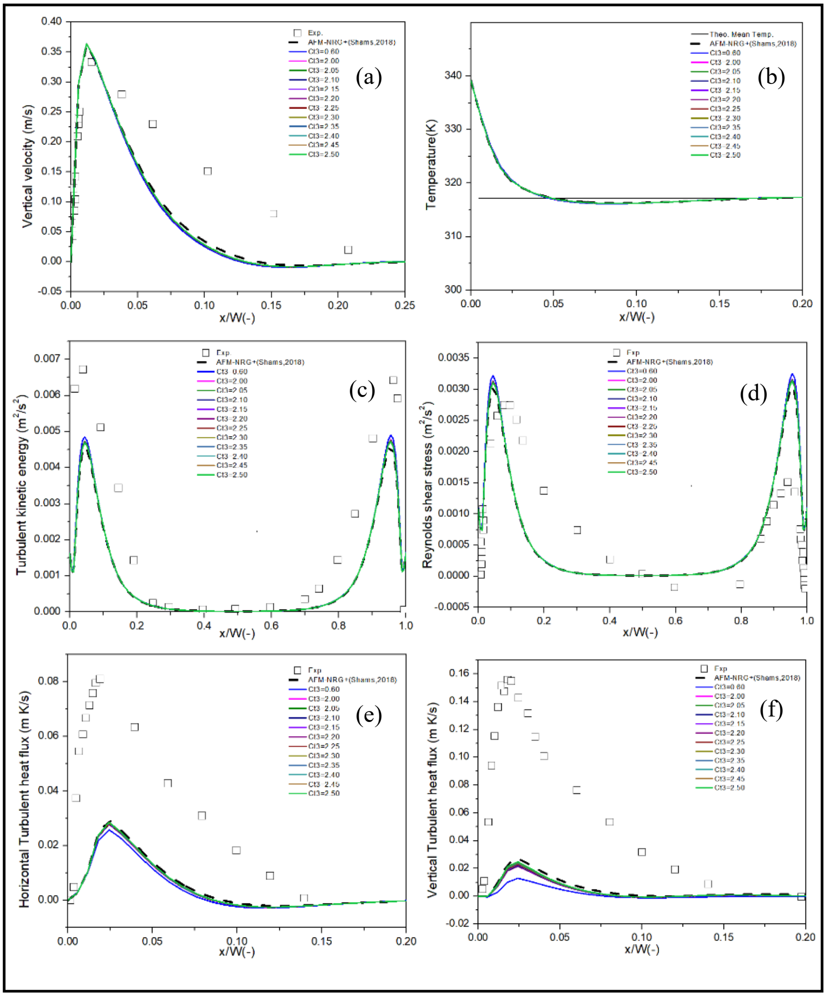


Figure 7. Sensitivity effect of $C_{t3}$ to the to the evaluated parameters (vertical velocity [a], temperature [b], turbulent kinetic energy [c], Reynolds shear stress [d], horizontal [e] and vertical turbulent heat flux [f]) measured through the mid-width (y/H = 1.25) of the cavity

Shams *et al*. (2014) have also reported that both $C_{t0}$ and $C_{t1}$ were calibrated to improve the prediction of forced convection scenarios. It was further verified in Figure 8, that when both $C_{t0}$ and $C_{t1}$ were increased, the following plot characteristics were observed: (1) the near-wall velocity profile yielded a reasonable agreement with the experimental data; (2) the plot did not cross below the theoretical mean temperature line, which signifies accuracy; (3) decrease of turbulent flow parameters in the near-wall regions; and (4) an increase in turbulent heat flux were observed.

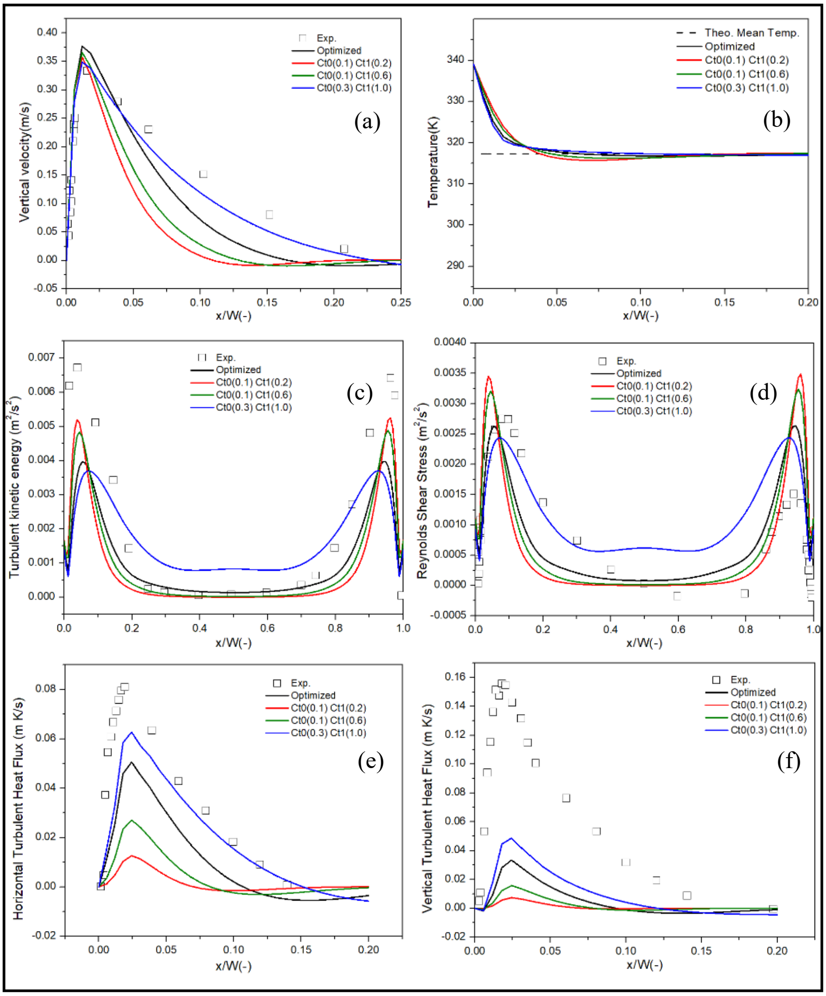


Figure 8. Sensitivity effect of $C_{t0}$ and $C_{t1}$ to the to the evaluated parameters (vertical velocity [a], temperature [b], turbulent kinetic energy [c], Reynolds shear stress [d], horizontal [e] and vertical turbulent heat flux [f]) measured through the mid-width (y/H = 1.25) of the cavity

However, when both $C_{t2}$ and $C_{t3}$ increased, only a slight difference can be found in turbulent intensity and heat flux parameters (Figure 9).

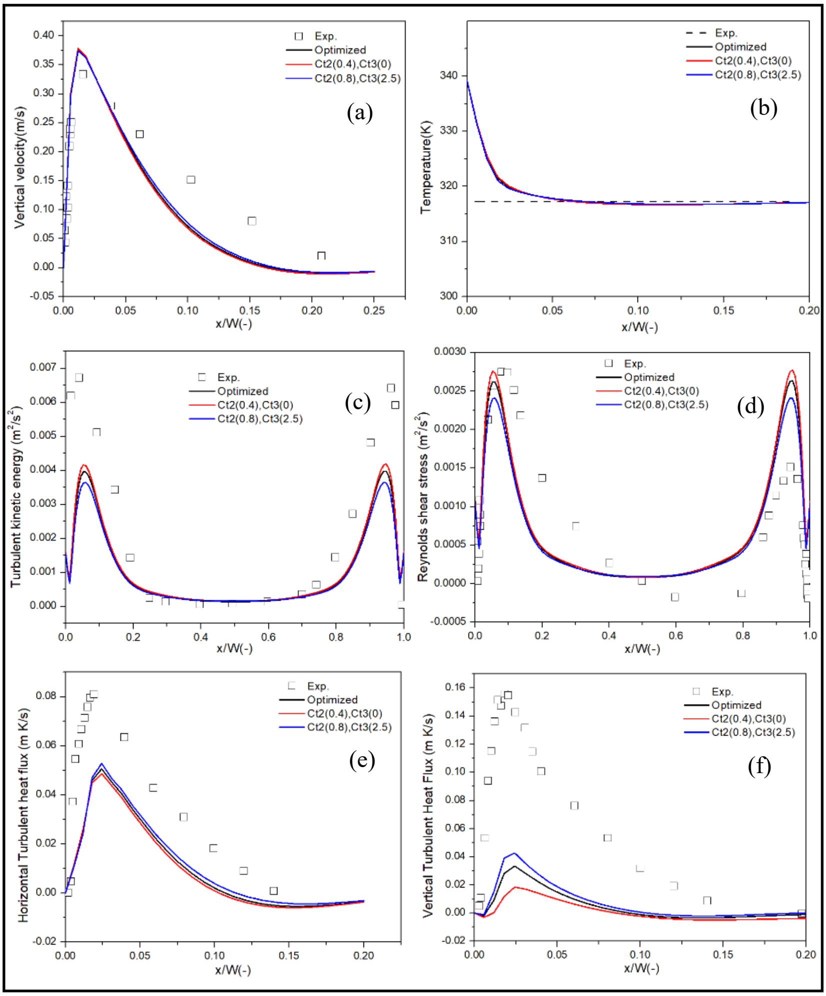


Figure 9. Sensitivity effect of $C_{t2}$ and $C_{t3}$ to the to the evaluated parameters (vertical velocity [a], temperature [b], turbulent kinetic energy [c], Reynolds shear stress [d], horizontal [e] and vertical turbulent heat flux [f]) measured through the mid-width (y/H = 1.25) of the cavity

From the parameter study of the AFM coefficients, the study confirmed that $C_{t0}$, $C_{t1}$ and $C_{t3}$ had a great influence on the prediction of turbulence data and the overall flow behavior, while $C_{t2}$ had little significance in buoyant and stratified conditions.

## 4. Conclusion and Recommendation

The first part of this study showed the potential of AFM in modeling turbulent flow and heat parameters compared with SGDH and GGDH as AFM was able to highlight turbulent fluxes in the neat-wall regions. The results from the recent modified versions of AFM improved the numerical predictability. NRG+ offered a balance between the turbulent stress and heat flux terms; hence, the most suitable for this case. The parameter study of $C_{t0}$, $C_{t1}$ and $C_{t3}$ demonstrated that the turbulence intensity was proportional to the coefficient. The term involving $C_{t1}$ was highly given importance for buoyant and stratified cases, which were the main features of the DHC case. The near-wall behavior can still be improved by using both grid convergence analysis and advanced artificial intelligence-based techniques for coefficient optimization.

For future work, experiments in liquid pools with representative geometry of the reactor lower head are much preferred to provide data on local heat flux distributions for reactor applications. Hence, the CFD simulation results of this configuration will shed more light on the turbulent convection phenomena of the corium.

## 5. Acknowledgement

This work was supported by Korea Hydro & Nuclear Power Co., Ltd (No. Safety 2-1: “High-Fidelity Numerical Analysis of Highly Turbulent Corium Pool for In-Vessel Retention (IVR) Strategy Feasibility Assessment”).

## 6. References

Cheesewright, R., King, K.J., & Ziai, S. (1986). Experimental data for the validation of computer codes for the prediction of two-dimensional buoyant cavity flows. Proceedings of ASME Meeting, Anaheim, California, 75-76.

Choi, S., & Kim, S. (2006). Computation of a turbulent natural convection in a rectangular cavity with the elliptic-blending second-moment closure. International Communications in Heat and Mass Transfer, 33(10), 1217-1224. https://doi.org/10.1016/j.icheatmasstransfer.2006.08.007

Choi, S., Kim, E., Wi, M., & Kim, S. (2004). Computation of a turbulent natural convection in a rectangular cavity with the low-Reynolds number differential stress and flux model. Korean Society of Mechanical Engineering International Journal, 18, 1782-1798. https://doi.org/10.1007/BF02984327

Choi, S., Han, J., Kim, S., & Lee, T. (2017). Computation of turbulent natural convection with the elliptic-blending differential and algebraic flux models. Numerical Heat Transfer, Part B: Fundamentals, 71(1), 37-49. https://doi.org/10.1080/10407790.2016.1257233

Davidson, L. (2021). Fluid mechanics, turbulent flow and turbulence modeling. Gothenburg, Sweden: Department of Mechanics and Maritime Sciences, Chalmers University of Technology.

Dinh, T.N., & Nourgaliev, R.R. (1997). Turbulence modelling for large volumetrically heated liquid pools. Nuclear Engineering and Design, 169(1-3), 131-150.

Hanjalić, K. (2002). One-point closure models for buoyancy-driven turbulent flows. Annual Review of Fluid Mechanics, 34, 321-347. https://doi.org/10.1146/annurev.fluid.34.082801.161035

Ji, Y. (2014). CFD modelling of natural convection in air cavities. CFD Letters, 6(1) 15-31

Kenjeres, S. (1998). Numerical modeling of complex buoyancy-driven flows (Dissertation). Delft University of Technology, Delft, Netherlands.

Ma, W., Yuan, Y., & Sehgal, B.R. (2016). In-vessel melt retention of pressurized water reactors: Historical review and future research needs. Engineering, 2(1), 103-111. https://doi.org/10.1016/J.ENG.2016.01.019

Peng, S.H., & Davidson L. (1999). Computation of turbulent buoyant flows in enclosures with low-Reynolds-number k-ω models. International Journal of Heat and Fluid Flow, 20, 172-184.

Shams, A. (2018). Towards the accurate numerical prediction of thermal hydraulic phenomena in corium pools. Annals of Nuclear Energy, 117, 234-246. https://doi.org/10.1016/j.anucene.2018.03.031

Shams, A., Roelofs, F., Baglietto, E., Lardeu, S., & Kenjeres S. (2014). Assessment and calibration of an algebraic turbulent heat flux model for low-Prandtl fluids. International Journal of Heat and Mass Transfer, 79, 589-601. https://doi.org/10.1016/j.ijheatmasstransfer.2014.08.018

Vieira, C.B., Ničeno, B., & Su, J. (2013). Computational simulation of turbulent natural convection in a corium pool. Proceedings of the 2013 International Nuclear Atlantic Conference, Recife, PE, Brazil, 1-15.

Whang, S., Park, H.S., Lim, K., & Cho, Y.J. (2019). Prandtl number effect on thermal behavior in volumetrically heated pool in the high Rayleigh number region. Nuclear Engineering and Design, 351, 72-79. https://doi.org/10.1016/j.nucengdes.2019.05.007